The Cryosphere Discuss., 4, 1365–1389, 2010
www.the-cryosphere-discuss.net/4/1365/2010/
doi:10.5194/tcd-4-1365-2010

The Cryosphere Discussions

Application of ground penetrating radar (GPR) in Alpine ice caves

H. Hausmann and M. Behm

Institute of Geodesy and Geophysics, Vienna University of Technology, Vienna, Austria

Received: 14 August 2010 – Accepted: 19 August 2010 – Published: 23 August 2010

Correspondence to: H. Hausmann (hausmann@mail.zserv.tuwien.ac.at)

Published by Copernicus Publications on behalf of the European Geosciences Union.

Abstract

Several caves in high elevated alpine regions host up to several meters thick ice fillings. The age of the ice may exceed some hundreds or thousands of years. However, structure, formation and development of the ice are not fully understood and are subject to relatively recent investigation. The application of ground penetrating radar (GPR) enables to determine thickness, volume, basal and internal structure of the ice fillings and provides as such important constraints for related studies. We present results from four caves located in the Northern Calcareous Alps of Austria and show that cave ice is far from being uniform. The transition from ice to the ground has variable reflection signatures, which is related to the deposit and size of debris. The internal structure of the ice fillings is characterized by banded structures which are inclined or parallel to the subsurface topography. These reflection signatures can result from thin layers of calcitic minerals and might help to understand the ice formation by representing isochrones.

1 Introduction

Ice caves are natural cavities with the occurrence of ice which persists for at least several years. Age, formation, development, conservation and degradation of the "underground ice" attracted scientific interest since the beginning of the 20th century and are also subject to relatively recent investigation (Luetscher, 2005, and references within). In 2006 a pilot study (AUSTRO*ICE*CAVES*2100) was started to encompass the above mentioned topics and primarily aims to fortify the basics and fundamental knowledge on ice caves. This includes the link between (Speleo-) meteorology and ice formation, determining the age of the ice as well as local quantification of ice volumes. Additionally, in regard to the current climate debates, the ice caves potential as possible climate archives should be investigated. The presented GPR data have been acquired in the course of this project.

TCD
4, 1365–1389, 2010

Based on the fact that underground ice exists for at least several years, it can be classified as a permafrost phenomenon. The application of geophysical methods to study glacial or frozen materials depends on the physical properties of earth materials which change with freezing of incorporated water and therefore the formation of varying amounts of ground ice. The relevant electrical parameters are resistivity (real or complex), relative permittivity, and loss tangent (Scott et al., 1990). Variation in these physical properties depends on unfrozen water content, air content, ice chemistry, and temperature conditions during permafrost genesis. EM (electrical and electromagnetic) techniques that operates at frequencies of a few Hz (e.g. D.C. resistivity sounding) are sensitive to the resistivity of materials whereas frequencies >100 kHz (e.g. GPR) are influenced by both resistivity and relative permittivity (Katsube et al., 1976).

We show that GPR can be successfully to map the thickness and structure of underground ice. This study documents the internal and basal structure of ice fillings in four different caves and highlight their pronounced differences. We further investigate particular features such as layering of the ice and relate them to the formation of ice.

2 Ice caves

Occurrence of extended ice fillings in caves results mainly from water which enters through the porous limestone. If the temperature is below zero, ice starts to form. Due to isolation by the surrounding rocks, the air temperature inside a cave is rather constant and equal to the annual average of the outside air temperature, and therefore, depends mainly on the elevation and geographic region. Additionally, most caves have more than one entrance and are ventilated. In summer, the relatively cold and heavy cave air sinks down and flows out at the lower entrances. In winter, this regime changes and relatively warm and light cave air leaves through the upper entrances. For compensation, cold outside air is sucked into cave at the lower entrances (Cigna, 2004). Cave ice grows therefore close to the lower entrances in winter and early spring when the outside temperature still is low and a lot of melt water enters the cave. On the

TCD
4, 1365–1389, 2010

other hand, the ice degrades in summer and autumn. Recent investigations (Delaloye and Lambiel, 2005; Phillips et al., 2009) found out that the formation of ice in ventilated talus slopes is controlled by a similar effect.

Heat exchange with the surrounding rocks and air, and sublimation are other factors controlling the dynamic behaviour of cave ice (Yonge, 2004). It is obvious that growth and degradation are very sensitive to (micro-)climatic changes. Ice caves are reliable environmental markers as their presence is controlled by specific climate conditions (e.g. winter precipitation, number of freezing days, MAAT; Luetscher, 2005). Nonlinear effects also play important roles: e.g., some entrances may be blocked by ice for a certain time and their opening changes the ventilation which in turn leads to ice growth and blockage of other entrances (Wimmer, 2008). Despite these various influences, we know from direct observation that massive ice bodies can pertain for at least hundred years. Dating of organic inclusions in ice caves yields ages up to 5180 (± 130) years (Achleitner, 1995). It is important to stress out the difference between seasonal ice (which completely disappears in summer and autumn and starts to form again in winter) and occurrences of ice bodies which exist for at least some decades. We only deal with the permafrost feature in this study.

Approximately 13 000 caves are currently known in the Northern Calcareous Alps (NCA) and about 900 of them comprise ice fillings (Stummer and Plan, 2002). On average, the ice filled parts are located in elevations ranging from 1300 to 2000 m a.s.l. We investigate the ice fillings of four caves (Fig. 1): Eisriesenwelt-Cave, Dachstein-Mammut-Cave, Dachstein-Rieseneis-Cave and Beilstein-Eis-Cave. For the first three caves, detailed descriptions of the field measurements and initial results (thickness) have already been published by Behm and Hausmann (2007, 2008). In the actual study, we apply advanced processing techniques (migration) and focus on the internal ice structure and the associated reflection signatures.

TCD
4, 1365–1389, 2010

3 Method

Ground penetrating radar (GPR) is geophysical method based on the propagation of electromagnetic waves (Davies and Annan, 1989). A short electromagnetic impulse of suitable center frequency is transmitted at the surface and the propagating wave is partially reflected at discontinuities of the medium's dielectric properties (e.g. permittivity and conductivity) (Robin et al., 1969). In a radargram the reflected energy from any subsurface target is recorded as function of time, amplitude and phase. If the radar velocity is known the correct position of subsurface targets can be imaged (migration) and converted from time to depth. This method is commonly employed to investigate the structure of the shallow underground.

Since the 1960s GPR is applied as a method for locating and mapping subglacial interfaces, and thereby to constrain ice volume and morphology (e.g. Robin et al., 1969; Arcone et al., 1995; Binder et al., 2009). In Woodward and Burke (2007) recent scientific advances to investigate hydrological, dynamic and thermal processes in glacial and frozen ground are discussed. Strong internal and basal reflectors can be derived from subglacial lakes and layers of firn, snow (Bingham and Siegert, 2007), sediments (Woodward et al., 2003) or debris (Arcone et al., 1995; Fukui et al., 2008). Changes in crystal-orientation fabric, changes in conductivity or changes in the amount of bubbles (respectively density) are also considered to cause internal reflections in glaciers and ice sheets (e.g. Harrison, 1973; Gudmandsen, 1975; Siegert, 1999; Eisen et al., 2007). Internal structures such as the dimension and water content of englacial channels are reported in Stuart et al. (2003).

The radar velocity in ice is mainly controlled by temperature, the orientation of ice crystals, the amount of water, air, chemical impurities, and sediment inclusions (Jezek et al., 1978; Macheret et al. 1993). Typical radar velocities are 0.167 m/ns for ice (Hubbard and Glasser, 2005), 0.033 m/ns for water, and 0.300 m/ns for air.

TCD
4, 1365–1389, 2010

Apart from our studies cave ice thickness measurements with GPR have been carried out in the Dobsinska ice cave (Slovakia) (Geczy and Kucharovic, 1995; Novotny and Tulis, 1995) and in Kungur Ice Cave (Russia) (Podshuhin and Stepanov, 2008).

4 Measurements and data processing

The applied system includes the GSSI SIR 2000 and 3000 instruments with shielded antennas ranging from 200 to 1200 MHz. In this study we concentrate on measurements from a shielded antenna with a center frequency of 500 MHz. However, in Dachstein-Rieseneis-Cave, large depths were expected and therefore a shielded 200 MHz antenna was applied. The measurements were carried out along crossing profiles in a continuous record mode. The main recording parameters were 2048 samples/scan, 16 bits/sample, and 64 scans/s. Taking the expected depths into account, the record lengths ranged between 100–400 ns. An electromagnetic pulse of 500 MHz propagates with a wavelength of 0.33 m in ice, which results in a vertical resolution of 0.08 m (1/4 of the signal wavelength). The horizontal resolution is a function of depth and the wavelength and is defined by the first Fresnel zone.

The raw data were processed with trace mixing (reduction of antenna noise), automatic gain control function (15 ns length), band pass-filter (250-350-700-900 MHz), migration (including velocity analyses), and static corrections using the 2-D software ProMAX (Landmark). Radar velocity was assessed by both reflection hyperbolae identified in numerous radargram sections and migration velocity analyses. The obtained velocities for the investigated ice fillings range from 0.160 to 0.165 m/ns (Table 1). No significant difference between the four caves could be ascertained. It has to be pointed out that the use of shielded antennae was crucial since the surrounding walls of the caves are strong reflectors. All discussed features were carefully examined with regard to their possible origins. Since we focus on the documentation and comparison of different ice fillings, the presented radargrams are consistently processed. We show both

TCD
4, 1365–1389, 2010

the unmigrated and migrated radargrams, and highlight details of characteristic internal and basal structures.

4.1 Dachstein-Mammut-Cave

Dachstein-Mammut-Cave has an overall passage length of 65 km and a vertical extension of 1207 m. Ice occurrences are located close to the western entrance, which is situated 800 m below the currently known highest entrances. The location "Feenpalast" (1360 m a.s.l.) is dominated by a 25 × 10 m wide and 3 to 4 m thick ice filling (Fig. 2a) which is relatively homogenous, and appears clear and diaphanous (Fig. 2e). Only a slight stratification is indicated by a variable content of millimetre-sized bubbles. The amount of embedded particles is generally low. However, layers with different grades of dispersal can still be discriminated. The underlying grounds consist of frozen clay (observed in January) and debris with a grain size of a few centimetres. A 17 m long profile was measured on top of the ice filling (Fig. 3a,b). The ice-ground transition is clearly visible in form of a continuous reflector. Weak sub-horizontal layering is seen above this reflector. Reflections from below the ice-ground transitions are attributed to structures within the frozen sedimentary underground.

Another 12 m long profile was obtained on a more than 9 m high ice cliff (Fig. 3c,d). At this location, the ice appears mostly intransparent and has only thin layers of clear ice (Fig. 2g). Additionally, numerous thin strata of a greyish to brownish particles are interposed. A similar stratum from Eisriesenwelt-Cave (see below; May et al., 2010) was analyzed and found out to be cryogenic calcite (Spötl, 2008, 2010, this issue). This form of calcite is produced by decarbonation when saturated water transforms to ice (Clarke and Lauriol, 1992). At the bottom, the ice transits into an ice-debris mixture. The radargram section shows very pronounced layering of the ice cliff. A multitude of reflection bands is visible down to depths of 4–6 m. Three prominent layers seen both on the side of the cliff and in the radargram section are highlighted in Fig. 3d. The strata of the thickest layer (5 mm) correlates with the identified calcitic minerals.

TCD
4, 1365–1389, 2010

A 40 m long profile was measured at the nearby location “Saarhalle” (Fig. 4) which comprises an ice filling with a 40 × 15 m wide planar surface. The maximum thickness of the ice is 6 m. At one side it is possible to access the ice-ground transition (in 4 m depth) which is dominated by large boulders (average sizes 1 to 2 m, Fig. 2b). Opposed to “Feenpalast”, the radargram section does not yield a continuous reflector at the bottom, but represents a series of reflection hyperbolae with mean wave velocities of 0.165 m/s. A remarkable feature are multiples of pronounced tilted reflection bands in the left part of the ice cliff which are also visible on interlocking profiles. Reflections from below the ice-ground transition are numerous and strong, and are attributed to either fissures in the bedrock or debris.

4.2 Dachstein-Rieseneis-Cave

Dachstein-Rieseneis-Cave is located close to Dachstein-Mammuthöhle. Its passage length is only 2.7 km, but ice covers almost half of the cave. A 20 m long profile was recorded with a 200 MHz antenna (Fig. 5) on a 50 m by 30 m wide ice filling. The elevation of this location is 1460 m a.s.l. An outcrop in the anterior part gives a first idea of the possible ice thickness, as debris is partly exposed on the ground and the maximum overall cave height is 20 m. In the vicinity of the profile, relatively large voids in the size of 1 to 2 m are molten out by episodic water channels and air currents (Fig. 2f). The lower boundary of the ice cliff is not clearly identifiable in the GPR data, but the maximum thickness seems to be between 13 m and 15 m. Between 3.5 and 5 m depth, short horizontal reflection bands can be identified. Compared to the other radargrams, several reflection hyperbolae (not superimposed on the layers) from within the ice body are observed. The distinct reflection hyperbola at 80 ns and 13 m profile distance most likely results from a relatively small boulder since in case of a larger void multiple reflections would be expected.

TCD
4, 1365–1389, 2010

4.3 Eisriesenwelt-Cave

The Eisriesenwelt-Cave has an overall passage length of 42 km. The only known entrance is located 1642 m a.s.l., and the ice part of the cave extends from there for almost 800 m. The "Eispalast" is an even ice surface at the end of the ice part with a slope of about 2°, a length of 50 m and a width of 8–20 m (1740 m a.s.l.). Ice thicknesses in the eastern part lie between 1.5 m and 2.5 m, while it rises quite sharply in the southern part to 7.5 m (Fig. 6). The reflecting horizon consists of numerous small reflection hyperbolae. This is in accordance with observations of the boulder size (on average 0.5 to 1 m) which constitute the ground at this location. Another interesting result are again multiples of slightly dipping reflection bands which traverse the entire ice filling. These well-visible layers can be identified down to 5 m depth. However, at this location the ice cannot be accessed from the side so the origin of these reflections cannot be ascertained so far.

4.4 Beilstein-Eis-Cave

Beilstein-Eis-Cave is located in the eastern part of the NCA at an elevation of 1330 m a.s.l. Opposed to the other ventilated caves, it represents a static ice cave. This type of ice caves exhibit only one (upper) entrance. Cold, heavy air sinks down into the cave in winter and is conserved throughout the summer. If the amount of cold air is large enough, negative temperatures and cave ice can persist throughout the year. A 30 m long profile was recorded on a planar ice surface (1320 m a.s.l., Fig. 7). The ice-ground transition is rather reflective in the right part and reveals a maximum ice thickness of about 10 m. It is known from surface observation that the ice filling partly lies on a sedimentary layer. Further, in the right part the radargram appears relatively transparent in the upper 2 to 4 m and more reflective below. The reflections represent both tilted layers and individual reflection hyperbolae. In contrast to the other caves, the layers are not as continuous.

TCD
4, 1365–1389, 2010

5 Results

5.1 Basal structure

Visual inspection of basal structures (Fig. 2) show that the transition from an ice filling to the ground involve substrates such as sediment and debris (from fine-grained up to boulders of several meters). Bedrock was never encountered. In general, the ice-ground transition recorded by GPR is characterized by a sudden increase in reflectivity and termination of the internal layers (Fig. 8). The transition to a fine-grained sedimentary underground is characterized by a short, high reflective, continuous reflector (Fig. 8a). The sediments are likely silts and clays with significantly higher permittivity than ice. Their origin is either dissolved limestone or remnants from glacial backfill. In contrast a basal structure composed of large boulders (>0.5 m) is identified by a large number of high reflective diffraction hyperbolae (Fig. 4a) and results in the characteristic signature shown as migrated section in Fig. 8b,c. It must be considered that the contrast in permittivity is relatively small between ice (3–4) and limestone (4–8) (Davis and Annan, 1989). In this case, the strong amplitude of the reflections may be caused by increased humidity or voids between ice and debris.

5.2 Internal structure

Visual inspection of the ice fillings in the Dachstein-Caves (Fig. 2) exhibit that fabrics (voids, particles, opaqueness) are significantly different at each location, and also change in vertical direction. Samples from the Dobsina cave (Clausen et al., 2006) reveal that intransparent, cloudy bands are caused by layers of small bubbles. They are the most common feature, but abundant brownish dark layers were also found. We also observe thin layers (up to 5 mm thickness) of particles (e.g. Fig. 2c). They most likely result from accumulation of cryogenic calcites (Clark and Lauriol, 1992) or dust resulting from "conventional" dissolution of limestone. The size of the observed voids ranges from millimetres to centimetres and are best described as elongated and

TCD
4, 1365–1389, 2010

rounded bubbles. Their infill could be unfrozen water or air. The strata of the ice filling in "Feenpalast" (Fig. 2d) show changes of the temporal evolution of ice formation. Subsurface parallel strata in the footwall and horizontal strata in the hanging wall indicate that the run-off of the seepage water changed. In Riesen-Eis-Cave large voids (>0.5 m, Fig. 2f) formed by episodic water channels and air currents were identified.

We observe different internal reflection signatures from the ice fillings (Fig. 9). Among them are tilted banded layers. Their inclination varies between almost horizontal and the slope of the sub-surface topography. The latter were observed at "Feenpalast" (Fig. 3b), at "Saarhalle" (Fig. 4b), and partially at the bottom at Beilstein-Eis-Cave (Fig. 7b). At "Eispalast" (Fig. 6b) the layers are almost horizontal despite a strongly inclined subsurface topography.

At all locations reflections caused by point sources (e.g., small boulders) were found. They are either superimposed on the layers (Fig. 9) or occur as individual reflections. The point sources associated with layers are separated by regular and irregular intervals. Only at the location "Eispalast" the layers appear without point reflectors, but the termination of the layer is indicated by a pronounced diffraction hyperbola.

At the location "Saarhalle" a curved structure is observed (Fig. 9d). Its origination is interpreted to be caused by subsurface undulation (e.g. a large boulder). Internal deformation of the ice would require a much higher load.

6 Conclusions

GPR in combination with shielded antennae has been proven to be well suited to investigate the thickness and volume of ice fillings in caves as well as to image their basal and internal structure. Centre frequencies between 200 and 500 MHz allow penetrating ice fillings of at least 10–15 m thickness. The interpreted ice thickness could be confirmed by core drilling (May et al., 2010; Kern et al., 2010) at the locations "Saarhalle" and "Eispalast". Reflection signatures show that both basal and internal structure of the ice is far from being uniform. The continuity of basal reflections and/or the extent

TCD
4, 1365–1389, 2010

of associated reflection hyperbolae correlate with the deposit and the size of the underlying debris. An internal structure characterized by multiples of pronounced tilted reflection bands was found in all ice fillings. These structures may contribute to understand processes involved with the formation of ice. The inclination of banded layers and its vertical variation can indicate changes in the run-off of seepage water. Further, the punctiform information gained from ice cores may be linked by observation of continuous internal layers (Eisen et al., 2003).

Accumulated layers of particles (sediments in general, cryogenic calcites) must represent isochrones (e.g. onset of accumulation after a period of degradation). These inclusions could produce the recorded reflection bands as the change in permittivity (ice: 3–4, clayish sediments: 5–40; Davies and Annan, 1989) is expected to be observable. We further believe that changes in amplitude along a reflection band (e.g. Figs. 3b, 7b) is rather caused by interbedded particles with different grades of dispersal than by changes in crystal-orientation fabric. This hypothesis is supported by the occurrence of reflections originating from a visible shallow sediment layer within the ice (Fig. 4).

Acknowledgements. Thanks go to the operators of the caves (Fam. Oedl & Austrian Federal Forestry AG), as well as the local cave guides (Alois Rettenbacher and Stephan Höll) for their special support and collaboration. Furthermore, we would like to thank all other staff at the caves and everyone who helped out during the surveys. Joanneum Research contributed towards the study by supplying the 200 and 400 MHz antennae. The dedication shown by Daniel Binder allowed efficient conduction of the GPR surveys and was also particularly helpful during the processing. The measurements and data interpretation were sponsored by the Austrian Academy of Sciences as part of the AUSTRO ICE CAVES 2100 project. We further thank Barbara May (Heidelberg University, Germany) and Zoltan Kern (Hungarian Academy of Sciences) for providing information on the ice core data. Photographs were kindly provided by Andreas Neumann, Gernot Weyss, and Robert Illnar.

TCD
4, 1365–1389, 2010

References

Achleitner, A.: Zum Alter des Höhleneises in der Eisgruben-Eishöhle im Sarstein (Oberösterreich), Die Höhle – Fachzeitschrift für Karst- und Höhlenkunde, 46(1), 1–5, 1995.

Arcone, S. A., Lawson, D. E., and Delaney, A. J.: Short-pulse radar wavelet recovery and resolution of dielectric contrasts within englacial and basal ice of Matanuska Glacier, Alaska, USA, J. Glaciol., 41(137), 68–86, 1995.

Behm, M. and Hausmann, H.: Eisdickenmessungen in alpinen Höhlen mit Georadar, Die Höhle – Fachzeitschrift für Karst- und Höhlenkunde, 1–4(58), 3–11, 2007.

Behm, M. and Hausmann, H.: Determination of ice thicknesses in alpine caves using georadar, edited by: Kadebskaya, O., Mavlyudov, B. R., and Pyatunin, M., Proceedings of the 3rd International Workshop on Ice Caves, Kungur, Russia, 70–74, 2008.

Binder, D., Brückl, E., Roch, K. H., Behm, M., and Schöner, W.: Determination of total ice volume and ice thickness distribution of two glaciers in the Hohen Tauern (Eastern Alps) by ground penetrating radar (GPR), Ann. Glaciol., 50(51), 71–79, 2009.

Bingham, R. G. and Siegert, M. J.: Radio-Echo Sounding Over Polar Ice Masses, J. Environ. Eng. Geoph., 12(1), 47–62; doi:10.2113/JEEG12.1.47, 2007.

Cigna, A. A.: Climate of caves, in: Encyclopedia of caves and karst science, edited by: Gunn, J., Fitzroy Dearbon, New York, USA, 229–230, 2004.

Clarke, I. D. and Lauriol, B.: Kinematic enrichment of stable isotopes in cryogenic calcites, Chem. Geol., 102, 217–228, 1992.

Clausen, H. B., Vrana, K., Hansen, S. B., Larsen, L. B., Baker, J., Siggaard-Andersen, M. L., Sjolte, J., and Lundholm, S. C.: Continental ice body in Dobsina Ice Cave (Slovakia) – Part II. – Results of chemical and isotopic study, in: Proceedings of the 2nd International Workshop on Ice Caves, edited by: Zelinka, J., Demanovska Dolina, Slovak Republic, 29–37, 2007.

Davis, J. L. and Annan, A. P.: Ground penetrating radar for high resolution mapping of soil and rock stratigraphy, Geophys. Prospect., 37, 531–551, 1989.

Delaloye, R. and Lambiel, C.: Evidences of winter ascending air circulation throughout talus slopes and rock glaciers situated in the lower belt of alpine discontinuous permafrost (Swiss Alps), Norsk Geogr. Tidsskr., 59, 194–201, 2005.

Eisen, O., Wilhelms, F., Nixdorf, U., and Miller, H.: Revealing the nature of radar reflections in ice: DEP-based FDTD forward modeling, Geophys. Res. Lett., 30(5), 1218, doi:10.1029/2002GL016403, 2003.

TCD
4, 1365–1389, 2010

Eisen, O., Hamann, I., Kipfstuhl, S., Steinhage, D., and Wilhelms, F.: Direct evidence for continuous radar reflector originating from changes in crystal-orientation fabric, The Cryosphere, 1, 1–10, doi:10.5194/tc-1-1-2007, 2007.
Fukui, K., Sone, T., Strelin, J. A., Torielli, C. A., Mori, J., and Fujii, Y.: Dynamics and GPR stratigraphy of a polar rock glacier on James Ross Island, Antarctic Peninsula, J. Glaciol., 54(186), 445–451(7), 2008.
Geczy, J. and Kucharovic, L.: Determination of the ice filling thickness at the selected sites of the Dobsinska ice cave, Ochrana ladovych jaskyn Zilina, 17–23, 1995.
Gudmandsen, P.: Layer echos in polar ice sheets, J. Glaciol., 15(73), 95–101, 1975.
Harrison, C. H.: Radio echo sounding of horizontal layers in ice, J. Glaciol., 12(66), 383–397, 1973.
Hubbard, B. and Glasser, N.: Field techniques in glaciology and glacial geomorphology, John Wiley & Sons, New York, USA, 2005.
Jezek, K. C., Clough, J. W., Bentley, C. R., and Shabtaie, S.: Dielectric permittivity of glacier ice measured in situ by radar wide-angle reflection, J. Glaciol., 21 (85), 315–329, 1978.
Katsube, T. V., Wadleigh, M., and Erickson, R.: Electrical properties of permafrost samples, Geol. Surv. Can. Paper 76-1C, 83–90, 1976.
Kern, Z., Fórizs, I., Molnár, M., and Nagy, B.: Isotope hydrological studies on the perennial ice deposit of Saarhalle, Mammuthöhle, Dachstein Mts, Austria. The Cryosphere, submitted, 2010.
Luetscher, M.: Processes in ice caves and their Significance for Paleoenvironmental Reconstructions, Phd-thesis, Universität Zürich, Swiss Institute for Speleology and Karst Studies (SISKA), 2005.
Luetscher, M., Bolius, D., Schwikowski, M., Schotterer, U., and Smart, P. L.: Comparison of techniques for dating of subsurface ice from Monlesi ice cave, Switzerland, J. Glaciol., 53(182), 374–384, 2007.
Macheret, Y. Y., Moskalevsky, M. Y., and Vasilenko, E. V.: Velocity of radio waves in glaciers as an indicator of their hydrothermal state, structure and regime, J. Glaciol., 39(132), 373–384, 1993.
May, B., Spötl, C., Wagenbach, D., and Dublyansky, Y.: First results from an ice core drilled to bedrock in the Eisenriesenwelt cave, Austria, The Cryosphere, submitted, 2010.
Novotny, L. and Tulis, J.: Ice filling in the Dobsina ice cave, Kras a jaskyne (Liptovsky Nikulas), 16–17, 1995.

TCD
4, 1365–1389, 2010

Phillips, M., Mutter, E. Z., Kern-Luetschg, M., and Lehning, M.: Rapid degradation of ground ice in a ventilated talus slope: Flüela Pass, Swiss Alps, Permafrost Periglac., 20(1), 1–14, 2009.

Podsuhin, N., and Stepanov, Y.: Measuring of the thickness of perennial ice in Kungur Ice Cave by georadar, edited by: Kadebskaya, O., Mavlyudov, B. R., Pyatunin, M., Proceedings of the 3rd International Workshop on Ice Caves, Kungur, Russia, 52–55, 2008.

Robin, G. D. Q., Evans, S., and Bailey, J. T.: Interpretation of Radio Echo Sounding in Polar Ice Sheets, 18 December 1969, Philos. T. Roy. Soc. Lond. A, 265, 437–505, doi:10.1098/rsta.1969.0063, 1969.

Scott, W. J., Sellmann, P., and Hunter, J. A.: Geophysics in the study of permafrost, in: Geotechnical and Environmental Geophysics, Vol. 1: Review and Tutorial, Society of Exploration Geophysicists Investigation in Geophysics no. 5, 355–384, 1990.

Siegert, M.: On the origin, nature and uses of Antarctic ice-sheet radio-echo layering, Prog. Phys. Geog., 23, 159–179, 1999.

Spötl, C.: Kryogene Karbonate im Höhleneis der Eisriesenwelt (Cryogenic carbonates in cave ice of the Eisriesenwelt), Die Höhle – Fachzeitschrift für Karst- und Höhlenkunde, 59(1–4), 26–36, 2008.

Stuart, G., Murray, T., Gamble, N., Hayes, K., and Hodson, A.: Characterization of englacial channels by ground-penetrating radar: An example from austre Brøggerbreen, Svalbard, J. Geophys. Res., 108(B11), 2525, doi:10.1029/2003JB002435, 2003.

Stummer, G. and Plan, L.: Handbuch zum Österreichischen Höhlenverzeichnis (Documenation for the Austrian cave cadastre), Speldok, Verb. Österr. Höhlenforscher, Wien, 2002.

Wimmer, M.: Eis- und Lufttemperaturmessungen im Schönberg-Höhlensystem (1626/300) und Modellvorstellungen über den Eiszyklus, (Ice and air temperature measurements in the Schönberg-Höhlensystem (Totes Gebirge, Austria) and a model of cyclic ice dynamics), Die Höhle, 59, 1–4, 13–25, 2008.

Woodmard, J. and Burke, M. J.: Applications of Ground-penetrating Radar to Glacial and Frozen Materials, J. Environ. Eng. Geoph., 12(1), 69–85, doi:10.2113/JEEG12.1.69, 2007.

Yonge, C. J.: Ice in caves, in: Encyclopedia of caves and karst science, edited by: Gunn, J., Fitzroy Dearbon, New York, USA, 435–437, 2004.

TCD
4, 1365–1389, 2010

Table 1. Summary of location type, ice thickness and volume, visual inspections and reflection characteristics for the internal and basal structures.

Location Elevation Ventilation type	Max. Thickness Volume	Internal reflections	Visual inspection of internal structures	Basal reflections	Visual inspection of basal structures	Velocity (m/ns)
Feenpalast 1360 m Dynamic	4 m not calculated	Weak sub-surface parallel reflection bands	Diaphanous ice, slight stratification, low particle content	Sharp, reflective and continuous	Clay and debris (<10 cm)	0.165
Before Saarhalle 1360 m Dynamic	>9 m not calculated	Multitude of sharp, strong, reflection bands	Intransparent ice, strata with cryogenic calcites	Not observed	Debris-ice mixture	0.160
Saarhalle 1360 m Dynamic	6 m ca. 3200 m^3	Strong, sharp, subsurface parallel, tilted layers (6°)	Diaphanous ice	Large hyperbolae	Large boulders (1–2 m)	0.165
Riesen-Eis-Cave 1460 m Dynamic	>15 m not calculated	Large hyperbolae, few horizontal layers	Large voids (1–2 m), intransparent ice	Not clear	Debris (<50 cm)	0.160
Eisriesenwelt 1740 m Dynamic	7.5 m ca. 3700 m^3	Sharp, strong, tilted layers (3°), not sub-surface parallel	Not accessible	Small hyperbolae	Debris (0.5–1 m) at the end of the profile	0.165
Beilstein-Eis-Cave 1320 m Static	11 m ca. 4000 m^3	Zones of increased reflectivity, tilted layers (up to 10°)	Intransparent ice (outcrop beside the profile)	Highly reflective, continuous in the right part	Sedimentary layer at the end of the profile	0.160

TCD
4, 1365–1389, 2010

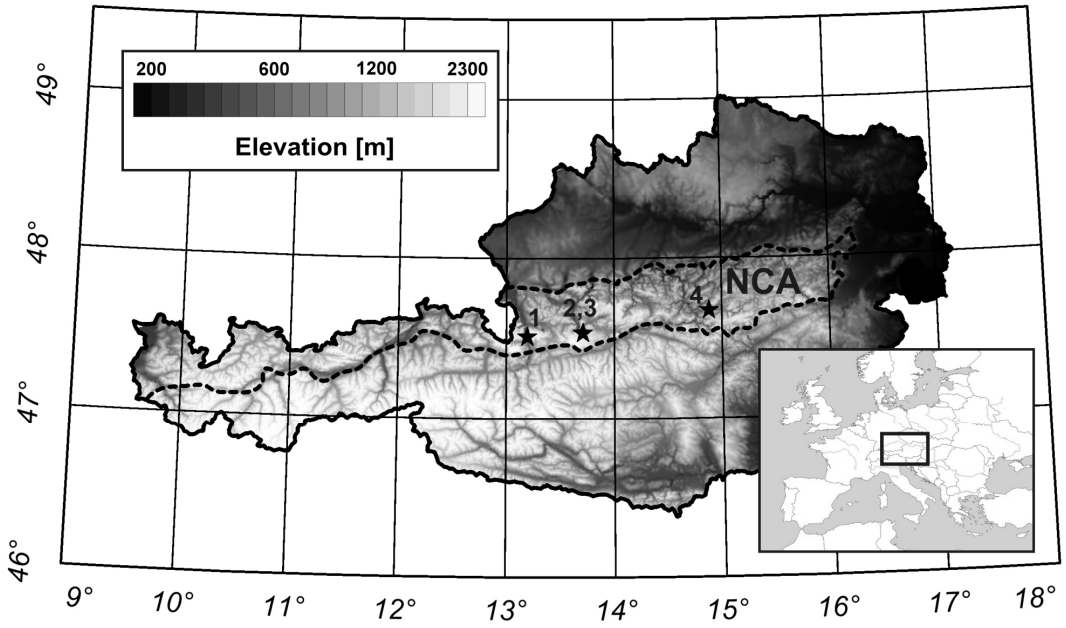

Fig. 1. Location of the investigated caves: 1 – Eisriesenwelt-Cave; 2, 3 – Dachstein-Mammut-Cave, Dachstein-Rieseneis-Cave; 4 – Beilstein-Eis-Cave. The broken line encompasses the Northern Calcareous Alps (NCA).

TCD
4, 1365–1389, 2010

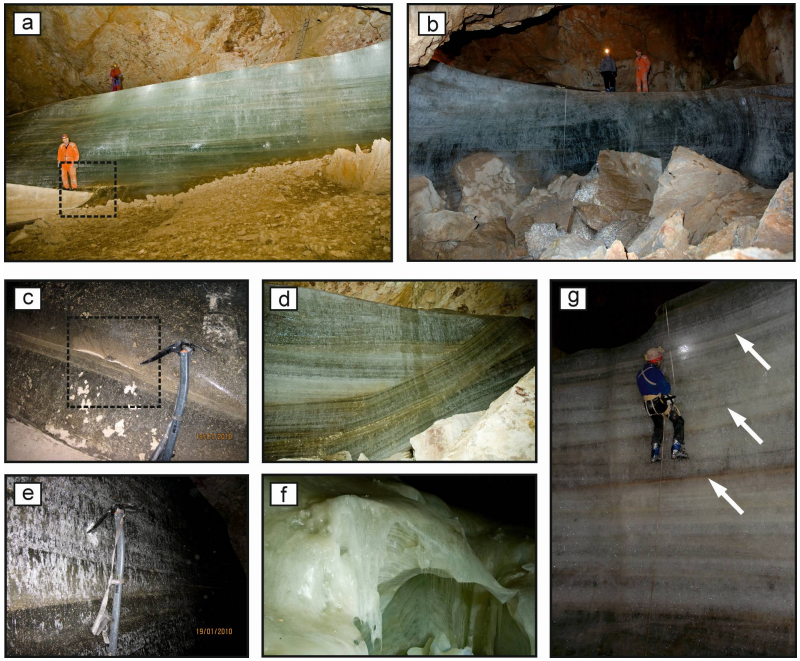

Fig. 2. Photographs of characteristic basal (a–b) and internal structures (c–g) found in the Dachstein-Caves. **(a)** The ice filling at "Feenpalast" (Mammut-Cave) with an interbedded boulder. The basal substrate consist of a fine-grained sediments. **(b)** The ice filling at "Saarhalle" (Mammut-Cave) with large boulders on the ground. **(c)** The diaphanous ice at "Feenpalast" with embedded thin layers of accumulated particles. A zone of high particle density is highlighted. **(d)** Subsurface parallel strata in the footwall and horizontal strata in the hanging wall found at "Feenpalast". **(e)** Detail of the diaphanous ice pictured in (a). Slight stratification is indicated by a variable content of millimetre-sized bubbles and a low amount of embedded particles. **(f)** The intransparent ice at Rieseneis-Cave with a hole (diameter ~2 m) which has been formed by episodic water channels and air currents. **(g)** Side view of the intransparent ice cliff at "Feenpalast" and three prominent layers also seen in the radargram.

TCD
4, 1365–1389, 2010

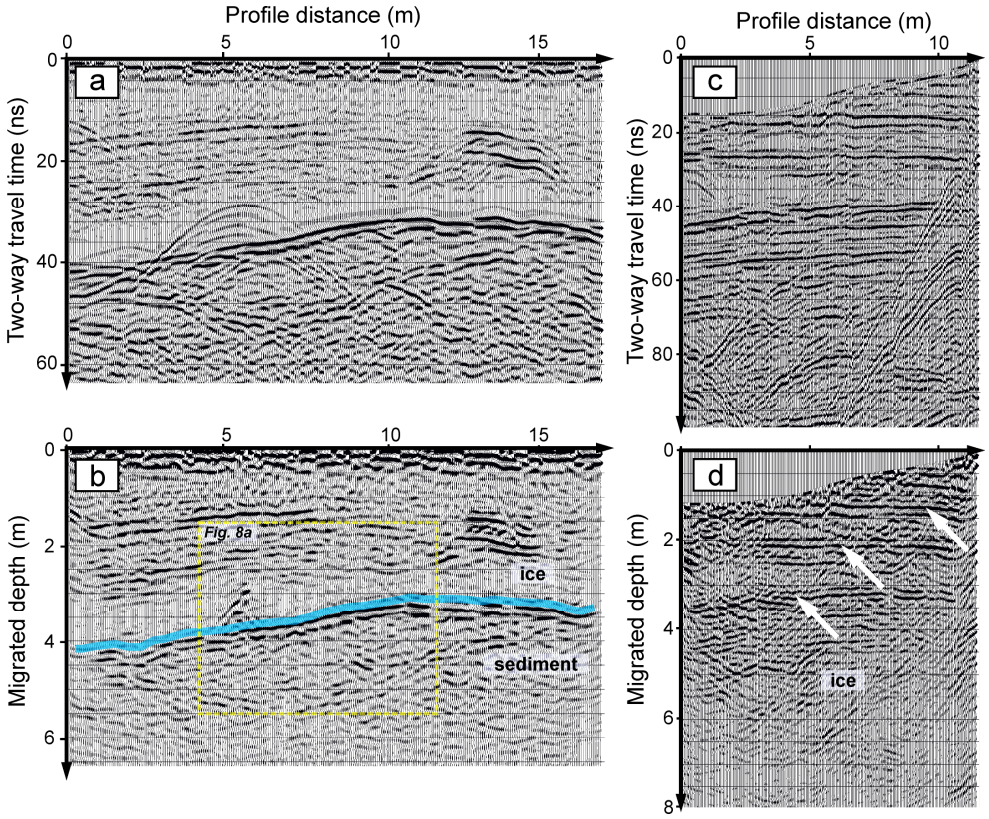

Fig. 3. Radargram sections of the ice filling (Fig. 2a) and the ice cliff (Fig. 2g) at "Feenpalast" (Dachstein-Mammut-Cave). **(a, b)** The fairly diaphanous ice filling clearly exhibit the transition from ice to the fine-grained sediment. The blue line in the migrated section (b) shows the ice-ground transition. **(c, d)** Radargram sections of the intransparent ice cliff with strata found close to the previous location. Solid line arrows indicate some of the prominent layers seen both on the side wall and in the radargram sections.

TCD
4, 1365–1389, 2010

Application of GPR in Alpine ice caves

H. Hausmann and M. Behm

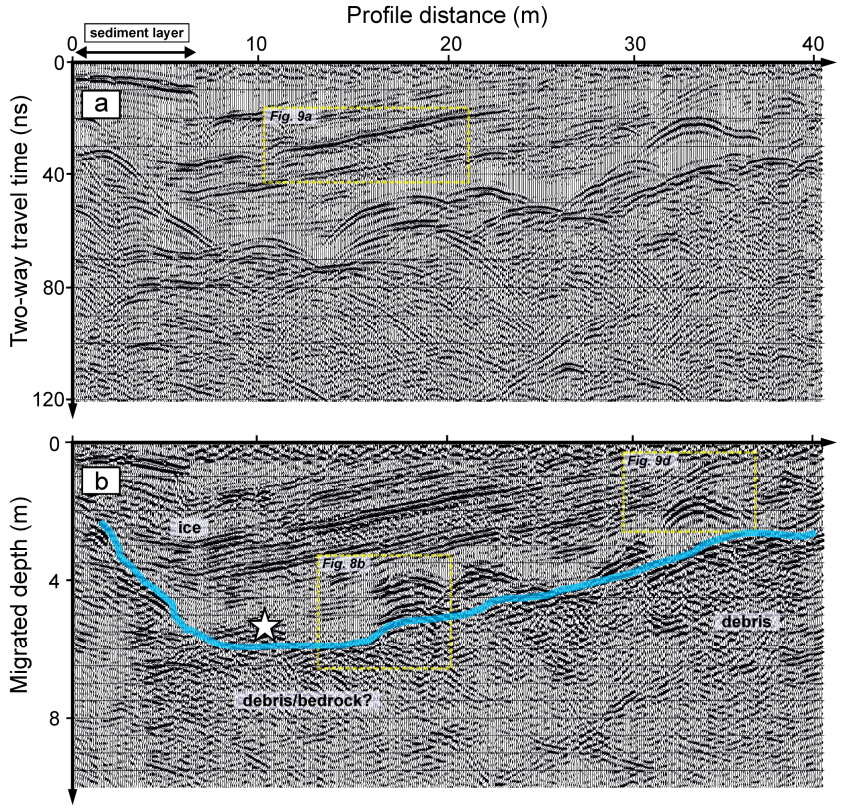

Fig. 4. Radargram sections from the location "Saarhalle" (Dachstein-Mammut-Cave). The white star indicates the maximum depth of a core drilling taken for isotopic analyses (Kern et al., 2010). The blue line in the migrated section **(b)** shows the interpreted ice-ground transition. Note the strong layering in inside the ice in the uppermost 4 m and the marked visible shallow sediment layer. Remarkable is the inclination of the internal layers which is parallel to the sub-surface topography. A picture of an outcrop which runs perpendicular to the GPR section at the profile distance of 30 m is shown in Fig. 2b.

TCD
4, 1365–1389, 2010

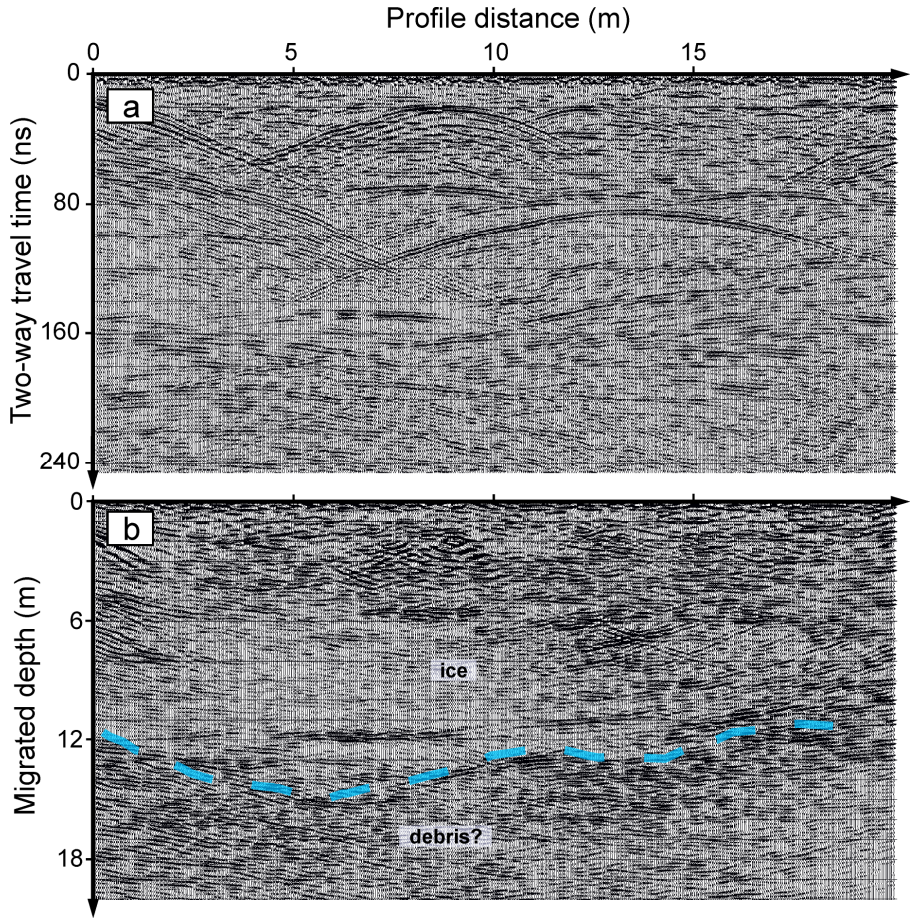

Fig. 5. Radargram sections from Dachstein-Rieseneis-Cave using the 200 MHz antenna. The base of the ice is better imaged in the migrated section. The blue line in the migrated section **(b)** shows the interpreted ice-ground transition.

TCD
4, 1365–1389, 2010

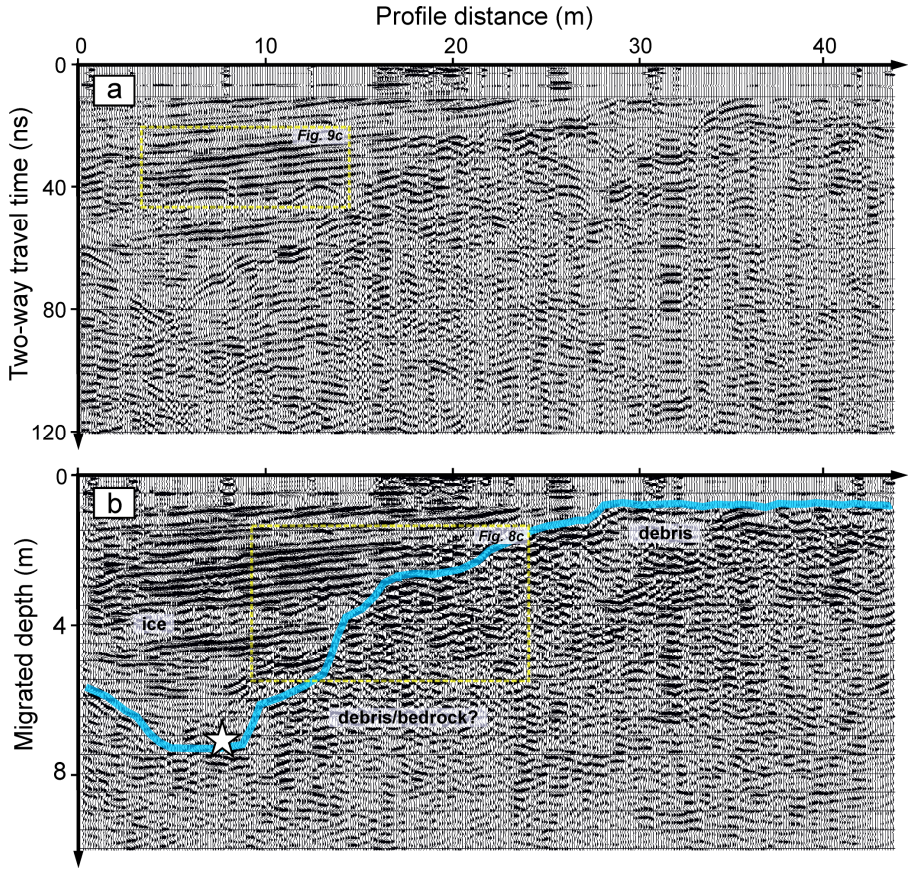

Fig. 6. Radargram sections from Eisriesenwelt-Cave. Note the strong layering in inside the ice in the first half of the profile. The blue line in the migrated section **(b)** shows the interpreted ice-ground transition. The white star denotes the maximum ice depth (7.3 m) from the core drilling reported in May et al. (2010). Note that the inclination of the internal layers do not follow the sub-surface topography.

TCD
4, 1365–1389, 2010

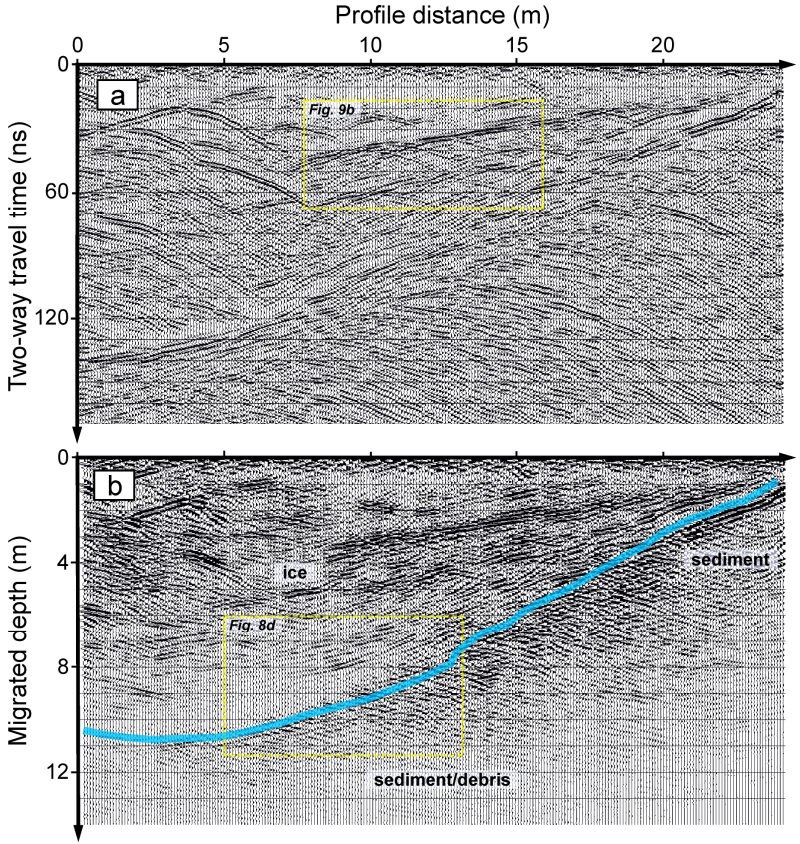

Fig. 7. Radargram sections from Beilstein-Eis-Cave. The blue line in the migrated section **(b)** shows the interpreted ice-ground transition. In the right part pronounced internal reflections represent both tilted layers and individual reflection hyperbolae. The inclination of the reflection bands varies between almost horizontal and the slope of the interpreted sub-surface topography.

TCD
4, 1365–1389, 2010

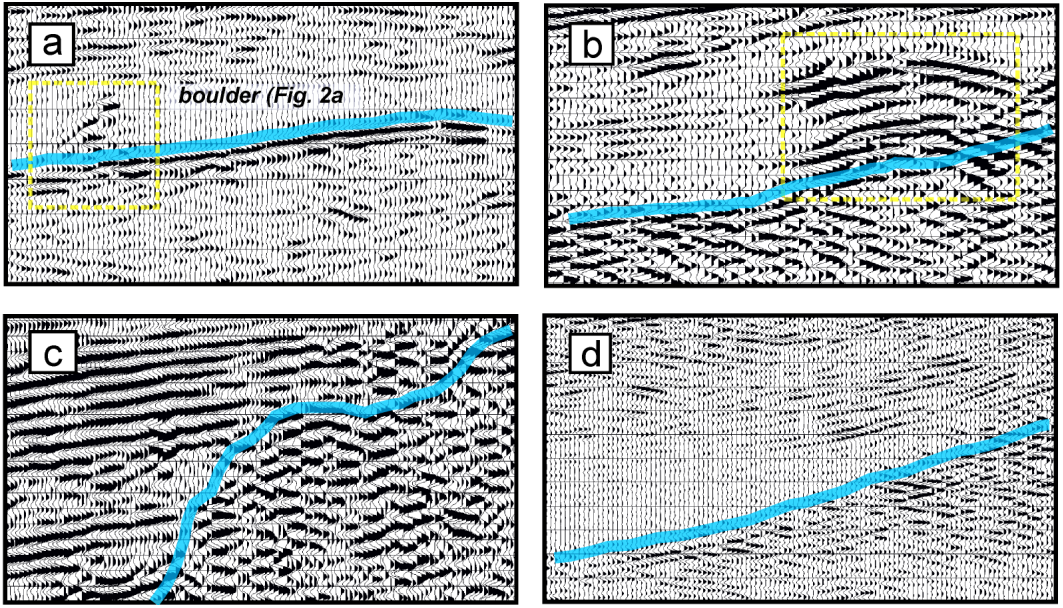

Fig. 8. Details from characteristic basal structures displayed as migrated sections. **(a)** The ice-sediment transition extracted from Fig. 3. The reflective zone in the left part originates from a large boulder. **(b)** Transition from ice to either debris or jointed bedrock. The reflection signature is generated by large boulders (Fig. 2b). **(c)** The extracted section from Fig. 6 exhibit an ice-ground transition characterized by the termination of internal layers. The chaotic returns from the ground originate from either debris or bedrock. **(d)** An ice-ground transition characterized by a sudden increase in reflectivity (see also Fig. 7). In the right part sub-surface parallel internal layers near the basal zone are identified.

TCD
4, 1365–1389, 2010

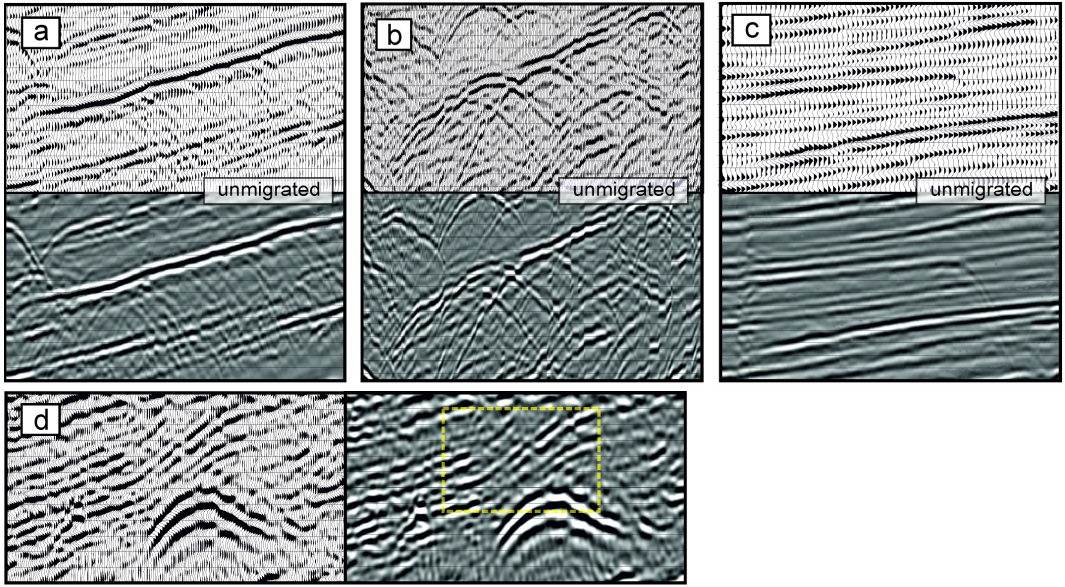

Fig. 9. Details from characteristic internal structures displayed in wiggle trace and variable density modus. **(a)** The detail of Fig. 4 show many point sources at regular interval superimposed on the banded layers. **(b)** Much less point sources occur at irregular intervals on the detail from Fig. 7. **(c)** The layers appear without point reflectors, but the termination of a layer is indicated by a pronounced diffraction hyperbola (see Fig. 6). **(d)** The curved structure imaged in Fig. 4 probable originates from an underlain boulder.

TCD
4, 1365–1389, 2010